ACS Biomaterials SCIENCE & ENGINEERING

pubs.acs.org/journal/abseba

Article

Protein Nanoparticles for Enhanced Oral Delivery of Coenzyme-Q10: *in Vitro* and *in Silico* Studies

Vanessa Jane Banun, Prarthana Rewatkar, Zanib Chaudhary, Zhi Qu, Taskeen Janjua, Anuja Patil, Yuao Wu, Hang T. Ta, Nidhi Bansal, Jared A. Miles, Benjamin P. Ross, Tushar Kumeria,* and Amirali Popat*

Cite This: *ACS Biomater. Sci. Eng.* 2023, 9, 2846−2856

Read Online

ACCESS | Metrics & More | Article Recommendations | Supporting Information

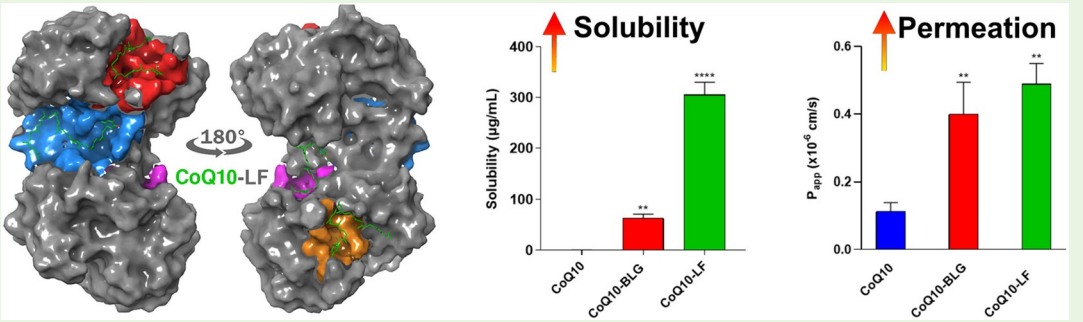

ABSTRACT: Coenzyme-Q10 (CoQ10) is a hydrophobic benzoquinone with antioxidant and anti-inflammatory properties. It is known to reduce oxidative stress in various health conditions. However, due to the low solubility, permeability, stability, and poor oral bioavailability, the oral dose of CoQ10 required for the desired therapeutic effect is very high. In the present study, CoQ10 is encapsulated into two milk derived proteins *β*-lactoglobulin and lactoferrin (BLG and LF) to produce self-assembled nanostructures of around 100−300 nm with high encapsulation efficiency (5−10% w/w). Both CoQ10-BLG and CoQ10-LF nanoparticles (NPs) significantly improved the aqueous solubility of CoQ10 60-fold and 300-fold, compared to CoQ10 alone, which hardly dissolves in water. Insight into the difference in solubility enhancement between BLG and LF was obtained using *in silico* modeling, which predicted that LF possesses multiple prospective CoQ10 binding sites, potentially enabling greater loading of CoQ10 on LF compared to BLG, which was predicted to be less capable of binding CoQ10. At pH 7.4, CoQ10-LF NPs showed a burst release between 30 min and 2 h then plateaued at 12 h with 30% of the total drug released over 48 h. However, pure CoQ10-BLG and pure CoQ10 had a significantly lower release rate with less than 15% and 8% cumulative release in 48 h, respectively. Most importantly, both BLG and LF NPs significantly improved CoQ10 permeability compared to the pre-dissolved drug across the Caco-2 monolayer with up to 2.5-fold apparent permeability enhancement for CoQ10-LF—further confirming the utility of this nanoencapsulation approach. Finally, in murine macrophage cells (J774A.1), CoQ10-LF NPs displayed significantly higher anti-ROS properties compared to CoQ10 (predissolved in DMSO) without affecting the cell viability. This study paves the way in improving oral bioavailability of poorly soluble drugs and nutraceuticals using milk-based self-assembled nanoparticles.

KEYWORDS: *Coenzyme Q10, Nutraceuticals, Ubiquinol, Ubiquinone, Lactoferrin, Self-assembled colloids, In silico modeling*

1. INTRODUCTION

Nutraceuticals such as resveratrol, curcumin, and coenzyme-Q10 (CoQ10) have garnered considerable attention in recent years due to their therapeutic effects, such as having antioxidant, anti-inflammatory, and anticarcinogenic properties.[1,2] CoQ10 is a hydrophobic benzoquinone with multiple potential therapeutic uses. Naturally, CoQ10 exists in humans in two redox forms known as ubiquinol and ubiquinone.[1] The role of CoQ10 in the management of Parkinson's disease,[3,4] cardiovascular diseases,[5] and statin-induced myopathy[6] has been widely investigated due to its strong antioxidant and anti-inflammatory properties. CoQ10 has been controversially classified as both a BCS Class II (high permeability but low solubility) and BCS Class IV drug (low solubility and low permeability) with limited oral bioavailability.[2,7] Widespread therapeutic application of orally delivered CoQ10 is restricted due to its low bioavailability and limited delivery into the systemic circulation.

Special Issue: Biomaterials for Oral Medicine

Received: September 11, 2020
Accepted: February 9, 2021
Published: February 22, 2021

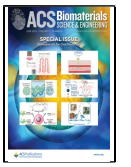

CoQ10 plays an essential role in the electron transport chain in mitochondria for ATP production;[2] therefore it is crucial in maintaining the functions of energy rich organs. CoQ10 supplements have been documented to improve the general well-being of the older population for their cardioprotective and hepatoprotective benefits.[8,9] However, CoQ-10 presents serious challenges in the development of oral formulation because of its high molecular weight (863 Da), light and temperature sensitivity, very high lipophilicity (log P = 21), and poor water solubility (<7 ng/mL), which reduce its absorption efficiency and bioavailability across the gastrointestinal tract (GIT).[2] It also has been approved for the treatment of mitochondrial disease by the United States Food and Drug Administration and is available in syrup (LiQ10) and softgel formulations (Q-Gel and Q-Nol).[10] However, these formulations use liposomes and/or oil to solubilize CoQ10. Although liposomes have been excellent in delivering drugs via a parenteral route, their applicability in oral dosage form has been limited due to their instability in the gastrointestinal tract, difficulties in crossing the gut membrane, and mass production problems leading to high cost associated with the formulations.[11] Current lipid or oil based formulations suffer from several challenges such as a moderate solubility of drugs leading to a high lipid to drug ratio, and highly concentrated formulations often lead to reprecipitation of the crystalline drug such as CoQ10 in the gut. Therefore, various formulation methods have been investigated to improve the solubility of CoQ10 including suspensions,[12] self-emulsifying methods,[13] nanoliposomes,[14] and nanoencapsulations.[15] However, these approaches require a stabilizer and surfactants, and the overall complexity of the formulation poses a challenge on the safety, toxicity, and cost-effective production of the final product.

Recently, food grade protein-based formulations have attained a lot of attention as alternative biomaterials for encapsulation and delivery of hydrophobic compounds including CoQ10.[16−20] Our recent study revealed that resveratrol can be efficiently encapsulated within milk protein β-lactoglobulin (BLG) with a high loading capacity and demonstrated improved anti-inflammatory properties in the murine model of colitis.[17] Nanoencapsulation using a solvent evaporation method has been proven to improve the solubility and stability of hydrophobic polyphenol such as resveratrol.[16,21] However, CoQ10 is a large molecule with high molecular weight (863 Da); therefore, in this study, we investigated two different proteins as encapsulants for CoQ10 and assessed their implications on the solubility, permeability, drug release, and antioxidant properties of CoQ10. BLG is derived from bovine milk and is widely found in the diet of a majority of the population. Milk based proteins are reported to enhance the delivery of phenolic nutraceuticals such as curcumin.[22,23] It is resistant to peptic enzyme degradation due to its highly charged amino acids, which prevents the cleavage of pepsin in its hydrophobic regions,[24] making it a potential candidate for CoQ10 encapsulation. Lactoferrin (LF) can be found in human saliva, tears, and bile; however, the major commercial source of LF is also milk.[25−27] LF has been proven to have oxide radical scavenging properties, antimicrobial activity, and anti-inflammatory activity.[26,28] It also plays a vital role in inhibiting proliferation of carcinoma cells when used to encapsulate polyphenol such as epigallocatechin gallate.[29,30]

We hypothesized that encapsulating CoQ10 in proteins BLG and LF nanoparticles (NPs; CoQ10-BLG and CoQ10-LF) will improve the solubility, stability, permeability, and dissolution of CoQ10. The CoQ10-protein NPs were evaluated for size, zeta potential, thermal behavior, infrared spectroscopy, loading efficiency, solubility, permeability, *in vitro* drug release, *in vitro* reactive oxygen species (ROS) assay, and *in vitro* Prestoblue cytotoxicity assay. *In silico* molecular modeling was also used to study the interactions between CoQ10 and the proteins, which elucidated the mechanism of CoQ10 encapsulation in BLG and LF. The results indicated that both proteins formed nanoparticles of size around 300 nm with good encapsulation efficiency. As evidenced by stronger and multisite binding, CoQ10-LF displayed significantly higher solubility compared to pure CoQ10 and CoQ10-BLG. CoQ10-LF NPs exhibited significantly higher solubility and dissolution of CoQ10 at pH 7.4 compared to CoQ10-BLG. Additionally, an *in vitro* permeability assay revealed that both types of nanoparticles improved CoQ10s permeability across the Caco-2 monolayer, confirming enhanced absorption. Finally, CoQ10-LF displayed significantly higher antioxidant properties compared to predissolved CoQ10 without affecting cell viability of J774A.1 cells *in vitro*.

2. MATERIALS AND METHODS

2.1. Materials. CoQ10 (Ubiquinone) was supplied by Blackmores Ltd. β-Lactoglobulin (BLG) from bovine milk, Dulbecco's modified eagle medium (DMEM), MEM nonessential amino acid solution (100×), bovine serum albumin (BSA), and 4-(2-hydroxyethyl)-piperazine-1-ethanesulfonic acid and N-(2-hydroxyethyl)piperazine-N′-(2-ethanesulfonic acid) (HEPES) were purchased from Sigma-Aldrich (Castle Hill, NSW, Australia). Lactoferrin (LF) from bovine milk was acquired from MG Nutritionals, Australia. Acetone was purchased from Merck (NSW, Australia). Acetonitrile and tetrahydrofuran used in loading analysis, solubility analysis, and the release study were of HPLC grade supplied by Merck (NSW, Australia). 2,7-Dichlorodihydrofluorescein diacetate (DCHF-DA) was purchased from Sigma-Aldrich (Castle Hill, NSW, Australia). Water used in all cell assays was Milli-Q water. Pen-Strep (penicillin 10 000 U/mL and streptomycin 10 000 μg/mL), Hank's balanced salt solution (HBSS), 0.25% Trypsin-EDTA (1×), L-glutamine (100×), and sodium pyruvate (100 mM) were from Gibco and Thermo Fisher Scientific, Australia. Phosphate buffered saline (PBS), RPMI 1640 medium, fetal calf serum, penicillin−streptomycin solution, and PrestoBlue cell viability reagent were purchased from ThermoFisher Scientific (VIC, Australia).

2.2. Methods. *2.2.1. Synthesis of CoQ10-Protein Nanoparticles.* CoQ10-NPs were synthesized using a slightly modified literature method.[16] The mass ratio of CoQ10/protein was kept at 1:9 (12 mg of CoQ10/108 mg of protein). The volume ratio of deionized water/acetone was kept at 1:1 (60 mL of deionized water/60 mL of acetone). Deionized water was used to dissolve proteins, whereas acetone was used to dissolve CoQ10. Protein solutions and CoQ10 solutions were left to mix separately on a magnetic stirrer at 700 rpm at room temperature and in a 37 °C temperature-controlled room, respectively, until all powder dissolved. CoQ10-acetone solution was added dropwise into the protein-deionized water solution, while the protein solution was mixed on a magnetic stirrer at 500 rpm in 37 °C temperature-controlled room. The CoQ10-protein solution was kept away from a light source. The solution was mixed overnight with a magnetic stirrer at 700 rpm in a 37 °C temperature-controlled room. Acetone was completely removed by rotary evaporation using a Buchi Rotavapor R-210 and Vacuum Controller V-850 at reduced pressure at 37 °C. The solution was frozen in a −80 °C freezer overnight prior to freeze-drying. Three batches of CoQ10-NPs were prepared for each protein type. Unloaded nanoparticles were prepared similarly without the addition of CoQ10.

2.2.2. Transmission Electron Microscope Imaging. The nanoparticles were observed under a transmission electron microscope (TEM). The samples were prepared in a 1 mg/mL water solution and adsorbed onto a copper TEM grid. The samples were then negatively

https://dx.doi.org/10.1021/acsbiomaterials.0c01354
ACS Biomater. Sci. Eng. 2023, 9, 2846−2856

stained with 2% uranyl acetate and imaged at 80 kV using HITACHI HT7700B TEM.[31]

2.2.3. Particle Size and Zeta-Potential. Particle size, polydispersity index (PDI), and zeta-potential were measured using a Malvern Zetasizer Nano-ZS, from ATA Scientific (Taren Point, Australia). Samples (0.1 mg/mL) were suspended in PBS (pH 7.4) and sonicated for particle size and zeta-potential measurement in a disposable folded capillary zeta cell (Malvern Instruments, DTS1060).

2.2.4. FTIR. Fourier transform infrared (FTIR) spectroscopy was performed using a PerkinElmer FT-IR UATR Two Spectrometer. The spectra were obtained for wavenumbers between 4000 and 400 cm^{-1}. Background spectra were scanned prior to analysis for each protein NP and Co-Q10.

2.2.5. DSC. Differential scanning calorimetry (DSC) was performed on a differential scanning calorimeter (TGA/DSC 2, Mettler Toledo, OH, USA). Approximately 3 mg of CoQ10, CoQ10-NPs, and unloaded NPs were weighed into an alumina crucible. An empty alumina pan was used as a reference. The samples were heated at a rate of 5 °C/min from 50 to 600 °C.

2.2.6. Quantitation of CoQ10 Using High Performance Liquid Chromatography (HPLC). For quantitative determination of CoQ10, a Shimadzu HPLC system consisting of a model FCV-10AL pump with a model SPD-20A UV detector was employed. The chromatographic separation was achieved using a 4.6 × 150 mm, 5 μm, C18(2), 100 Å Luna C18 analytical column (Phenomenex). The isocratic mobile phase consisted of acetonitrile/tetrahydrofuran (60:40 v/v). The isocratic elution profile was adopted for 0 to 10 min with a flow rate of 0.7 mL/min, and 10 μL of each sample was injected for chromatographic separation. For HPLC/DAD, each sample was chromatographed, and CoQ10 was measured at 275 nm wavelength. Retention times of separated peaks and the area under the peak data were recorded. Using the above method, a calibration curve was prepared for CoQ10 ranging from 100 ng/mL to 30 μg/mL (R^2 = 0.999).

2.2.7. Loading Efficiency (LE). Approximately 1 mg of samples was weighed into an Eppendorf tube, and then 2 mL of HPLC grade methanol was measured into respective samples. Each sample was dispersed using a vortex mixer until dispersed. Samples were placed on Ratek VM1 suspension mixer in a 37 °C room overnight, and centrifuged for 20 min at 20238*g* using a ThermoFisher Eppendorf Centrifuge 5424. Supernatant was transferred to a new Eppendorf tube. The remaining pellet was redispersed in 1 mL of HPLC grade methanol, then placed on suspension mixer in a 37 °C room for 30 min. The resulting suspension was centrifuged for 20 min at 20238*g*; then the supernatant was collected. All supernatants were collected and stored at −20 °C until ready for HPLC analysis. Loading efficiency was calculated using the following equation.

$$\%\mathrm{LE} = \frac{(\text{Initial conc.} - \text{Final conc.})}{\text{Initial conc.}} \times 100 \quad (1)$$

2.2.8. In Silico Computer Modeling. All computer modeling studies were performed using Schrödinger's Small Molecule Drug Discovery Suite (version 2019−2). The X-ray crystal structure of diferric bovine LF (PDB ID 1BLF)[32] and bovine BLG (PDB ID 3NPO)[33] were processed using the Protein Preparation Wizard to remove water, optimize hydrogen bonding, and minimize the protein structure using the OPLS3e force field, which has been demonstrated to deliver state of the art performance in protein simulations.[34,35] Potential binding sites on the protein were identified using SiteMap and chosen based on SiteScore.[36] This score is a function of the size, accessibility, charge, and interaction capabilities of a site. Grids for molecular docking were positioned and sized individually using the sites identified by SiteMap. The chemical structure of CoQ10 was prepared and minimized using LigPrep and then docked into each grid using Glide extra-precision (XP) molecular docking.[37] Docking poses and ligand−protein interactions were viewed in Maestro.

2.2.9. Solubility. CoQ10 (0.5 mg) and CoQ10 loaded protein nanoparticles (CoQ10-BLG and CoQ10-LF) containing an equivalent dose of CoQ10, were dispersed in 0.5 mL of deionized water respectively in separate microtubes. Solutions were placed on a suspension mixer and left to mix for 48 h in a 37 °C temperature-controlled room. Then, the solutions were centrifuged at 20238*g* for 20 min, and the supernatant was collected with new microtubes. The supernatant was centrifuged again at the same speed for 20 min, and the subsequent supernatant was collected and stored at −20 °C until ready for HPLC analysis. CoQ10 supernatants were analyzed without dilution; CoQ10 loaded NPs were diluted 10 times before analysis.

2.2.10. In Vitro Release Study. CoQ10-BLG and CoQ10-LF nanoparticles equivalent to 0.5 mg of CoQ10 were dispersed in 2 mL of PBS (pH 7.4) and spun on a rotary mixer in temperature-controlled room at 37 °C. One milliliter of the solution was extracted at predetermined time points and was centrifuged for 6 min at 20 238*g*. The supernatant was transferred to a new microtube. The remaining pellets were redispersed with fresh PBS solution and returned to the original 1 mL solution. This was repeated for various time points of 0.5, 1, 2, 4, 8, 12, 24, and 48 h. Pure CoQ10 (0.5 mg) was assessed under the same conditions as a control. Supernatants were stored at −80 °C in a freezer until ready for analysis using HPLC. CoQ10 supernatants from both NPs were diluted 10 times, whereas CoQ10 control was diluted 5 times with mobile phase solvent (ACN/THF; 60:40 v/v), then centrifuged for 6 min at 20238*g* to obtain supernatants prior to analysis.

2.2.11. Cell Culture. Macrophage J774A.1 and Caco-2 were obtained from the American Type Culture Collection (ATCC). Macrophage J774A.1 cells were maintained in a nontreated 100 × 20 mm cell culture dish containing RPMI 1640 with fetal calf serum (10%), penicillin (100 U/mL), and L-glutamine (1%) and cultured in an incubator at 37 °C with 5% CO_2. Caco-2 cells were maintained in a 12 well plate transwell DMEM with fetal calf serum (5%), penicillin (100 U/mL), L-glutamine, and sodium pyruvate (1%) MEM nonessential amino acid solution and cultured in an incubator at 37 °C with 5% CO_2.

2.2.12. In Vitro Permeability Assay. The *in vitro* permeabilities of CoQ10 and CoQ10NPs were determined by using a Caco-2 cell (P-9) monolayer assay. Caco-2 cells were seeded at a density of 1×10^5 cells/well in 12 trans-well insert (0.4 μm pore diameter, 1.12 cm^2 area; Corning Inc., Kennebunk, ME, USA) plates and were grown in DMEM supplemented with 10% fetal bovine serum (FBS) + 1 vol/vol% each of glutamine, pen−strep, MEM nonessential amino acids, and sodium pyruvate solution until the transepithelial electrical resistance (TEER) value reached 200−300 Ω cm^2. TEER measurements were recorded using an electrode connected to a Millicell ERS-2 V-Ohm Meter (Merck, Australia). Once the TEER value reached >200 Ω cm^2, the cells were washed with 1× Hank's balanced salt solution (HBSS; 0.5 mL). The permeability studies were performed by adding 0.5 mL of CoQ10 predissolved in 0.5% DMSO diluted with HBSS. A total of 0.5 mL of Lf-CoQ10 and BLG-CoQ10 NPs (equivalent to 50 μg/mL CoQ10) were dispersed in HBSS in the apical compartment of the insets, and HBSS and 0.5% DMSO-HBSS were used as controls. The basolateral compartment (receiver compartment) was filled with 1.2 mL of HBSS, and 0.3 mL of 10 mM HEPES/1% BSA solution. After 2 h samples from the basolateral compartment were withdrawn and extracted using ethanol and centrifuged twice at 20 238*g* for 10 min, the amount of CoQ10 present in the supernatant (receiver compartment) was determined by HPLC.[38,39] [Acetonitrile/acetic acid aqueous solution (5%; 50:50) was used as a mobile phase with flow rate of 1 mL/min at 25 °C, injection volume was 10 μL, and all the samples were analyzed at 275 nm.]

Apparent permeability coefficient (P_{app}) was calculated[40] by using following equation:

$$P_{app} = \frac{dQ}{dt} \times \frac{1}{C_o A} \quad (2)$$

where dQ/dt is the amount of CoQ10 (μg) present in the receiver compartment per time unit (s), C_o is the initial concentration of CoQ10 in the apical compartment (μg/mL), and A is the surface area of the Caco-2 cell monolayer (1.12 cm^2).

2.2.13. In Vitro Cytotoxicity Assay—Prestoblue. J774A.1 cells were detached with a cold medium when the cell confluence reached approximately 85%. Then, the cells were seeded into a 96-well plate at a density of 10 000 cells/well. After 24 h of incubation, the cells were treated with LF and CoQ10-LF equivalent to 5, 10, 15, 20, and 25 μg/

https://dx.doi.org/10.1021/acsbiomaterials.0c01354
ACS Biomater. Sci. Eng. 2023, 9, 2846−2856

Table 1. Z-Average, PDI, Intensity Mean Size, and Zeta Potential of Blank Protein Nanoparticles, and CoQ10-Protein Nanoparticles (Z-Average and PDI Calculated Using Cumulant Method and Intensity Mean Sizes Calculated Using Distribution Method)

sample	Z (average; nm) ± SD	intensity mean size (nm) ± SD	PDI ± SD	zeta potential (mV) ± SD	LE (%) ± SD
CoQ10	1921.00 ± 528	1818.00 ± 753	0.58 ± 0.06	−15.10 ± 0.21	
BLG	391.70 ± 54	738.70 ± 96	0.71 ± 0.13	−9.36 ± 0.43	
LF	280.10 ± 9	256.40 ± 143	0.68 ± 0.13	−2.13 ± 0.30	
CoQ10-BLG	386.07 ± 129	269.53 ± 24	0.48 ± 0.22	−11.63 ± 1.27	62.79 ± 4.13
CoQ10-LF	259.77 ± 24	258.80 ± 26	0.30 ± 0.04	−3.73 ± 0.19	86.77 ± 11.15

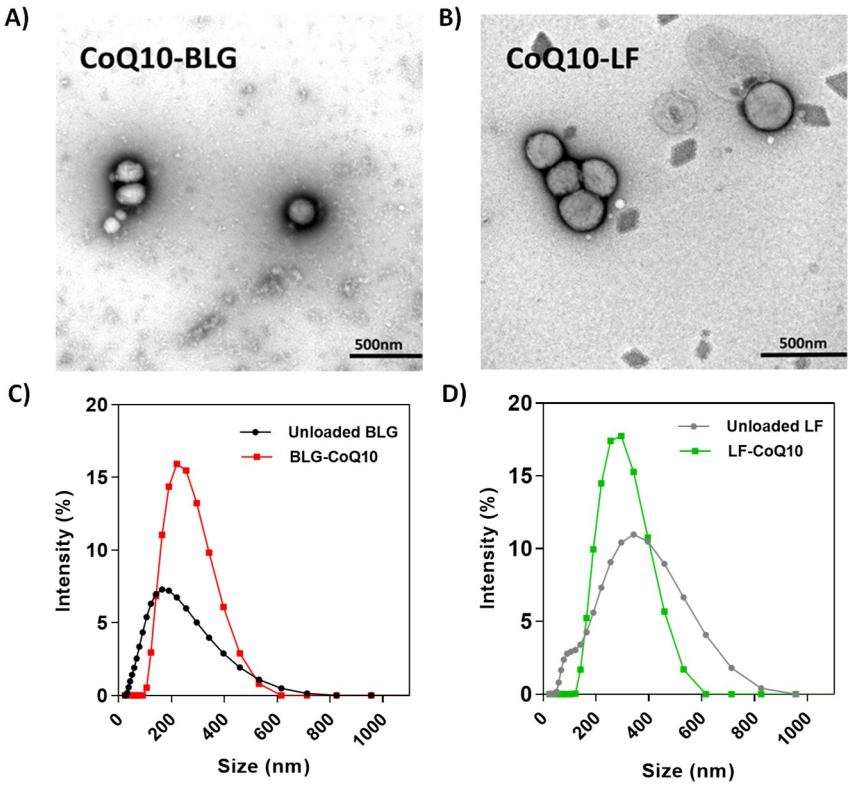

Figure 1. (A, B) Transmission electron microscope (TEM) images (scale bar is as shown in the image). (C, D) Particle size distribution using DLS.

mL CoQ10 for another 24 h. Then, cells were treated with 10 times diluted PrestoBlue cell viability reagent for 30 min. Fluorescence intensity was measured by plate reader (PerkinElmer) at an excitation wavelength of 535 nm and an emission wavelength of 615 nm. All experiments were performed in triplicate.

2.2.14. In Vitro anti-ROS Assay. Cells were detached using a cold medium when cell confluence reached approximately 85%. Then, cells were seeded into a 96-well plate at a density of 10 000 cells/well. After 24 h of incubation, the cells were treated with 5, 10, 15, 20, and 25 μg/mL CoQ10, CoQ10-LF equivalent to the CoQ10 concentrations, and unloaded LF nanoparticles as controls for another 24 h. Then, the cells were treated with 25 μM of DCHF-DA for 45 min following a one time PBS wash. After that, the cells were treated by 0.5 mM of H_2O_2 for 20 min. ROS inside the cells were detected by the fluorescence of DCHF. The fluorescence intensity was measured by PerkinElmer at the excitation wavelength of 485 nm and the emission wavelength of 535 nm. Fluorescence images were taken by a Nikon ECLIPSE Ti microscope system with Photometrics CoolSNAPTM HQ2 camera and Nikon INTENSILIGHT C-HGFIE fluorescent light source. All experiments were performed in triplicate.

3. RESULTS AND DISCUSSION

3.1. Physicochemical Characterizations. CoQ10-NPs and unloaded NPs were measured for particle size and zeta potential in PBS (pH 7.4) as shown in Table 1. All CoQ10-NPs have an average size (Z-avg) in the nano range compared to pure CoQ10 in the micron range. The Z-avg size of CoQ10-NPs was slightly smaller but not significant compared to unloaded NP for the respective protein types. The average diameter size of CoQ10-LF (259 ± 24 nm) is smaller, whereas CoQ10-BLG had a bigger diameter size (386 ± 129 nm) with a larger standard deviation. This could be potentially due to poor binding of CoQ10 with BLG and a difference in aggregation behavior of both proteins. It is important to note that the intensity mean diameter of BLG is much higher compared to CoQ10-BLG, which may be attributed to stabilization of the BLG aggregates due to complexation with CoQ10.[17] However, there is no difference in intensity mean or Z-Avg between LF and CoQ10-LF. CoQ10-LF was also more monodispersed with a PDI of 0.30, lower PDI means that the nanoparticles are better-dispersed and less likely to aggregate.[17] The PDI for the CoQ10-NPs were lower than respective unloaded NP which demonstrates that CoQ10 plays a significant role in improving the colloidal behavior and of protein NPs.[16,17] CoQ10-protein NPs possess greater negative zeta-potential compared to their respective unloaded NP counterparts. The zeta potential of CoQ10-BLG was more negative (−11.63 mV) compared to CoQ10-LF (−3.73 mV). Proteins and CoQ10 are anionic, thus

https://dx.doi.org/10.1021/acsbiomaterials.0c01354
ACS Biomater. Sci. Eng. 2023, 9, 2846−2856

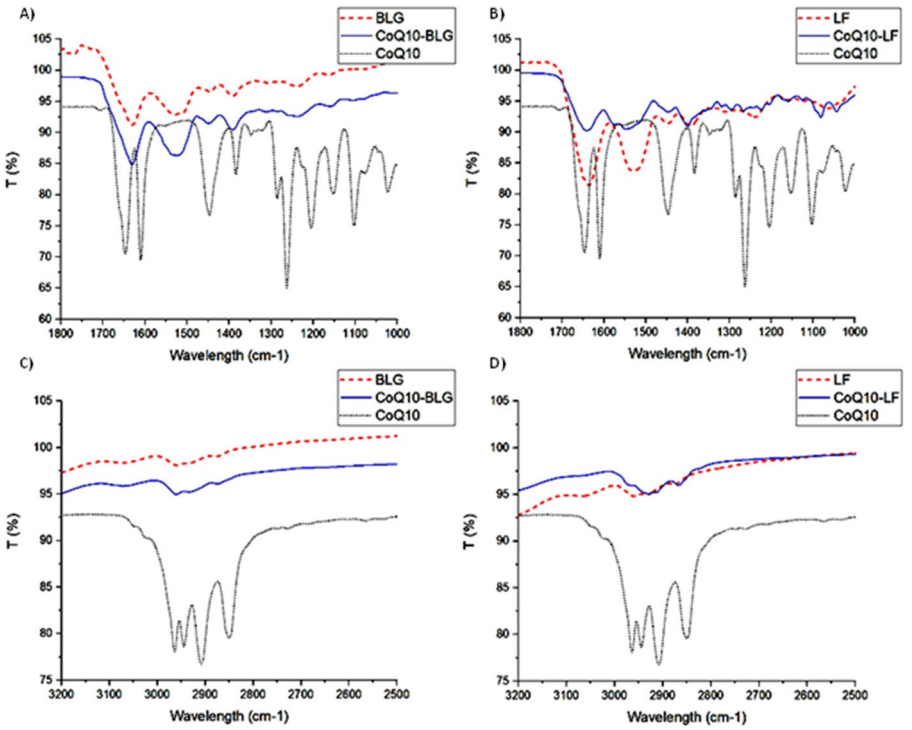

Figure 2. Fourier transform infrared (FTIR) spectroscopy analysis: (A,B) FTIR of BLG and LF NPs for the range 1000−1800 cm^{-1}. (C,D) FTIR spectra for respective NPs for the range 2500−3200 cm^{-1}.

a overall negative surface charge was observed for both protein NPs. The sizes of the CoQ10-NPs were much smaller in TEM (Figure 1A,B) than the hydrodynamic size of the nanoparticles as determined by dynamic light scattering (DLS; Figure 1C,D). DLS measures the fluctuation of scattering intensity of particles in Brownian motion and usually reports a greater size compared to other methods such as TEM.[41] The larger hydrodynamic size in DLS may also be caused by the aggregation of NPs in the aqueous state, therefore giving the diameter size of NP complexes. These results are consistent with our previous studies on soy protein isolate and BLG.[16,17]

FTIR spectroscopy data of CoQ10-NPs were compared against those of pure CoQ10 and unloaded protein NPs. CoQ10-NPs showed characteristic peaks of both CoQ10 and protein NPs, as seen in Figure 2. The spectra of CoQ10-BLG and CoQ10-LF (Figure 2A,B) showed peaks at 1648 and 1610 cm^{-1}, which correspond to a benzoquinone ring that appears to merge and form a wider band after encapsulation. Changes in the C−H stretching region can be observed between 2800 and 3000 cm^{-1} (Figure 2C,D). The peaks between 2900 and 2950 cm^{-1}, characteristic of CoQ10 merged into one peak, were consistent with the previous literature.[42]

DSC analysis on the CoQ10-NPs investigates the crystallinity of CoQ10 in protein nanoparticles. A melting peak of CoQ10 was obtained at around 50−55 °C as shown in Figure 3, but no peak was observed with all CoQ10-NP formulations. These results indicated that CoQ10 existed in an amorphous state upon encapsulation in BLG and LF.

3.2. *In Silico* Modeling. SiteMap identified four potential CoQ10 binding sites on the surface of LF (SiteScores ≥ 1.00), and CoQ10 docked favorably into each of these sites based on XP GlideScores, which approximate ligand-binding free energy (Figure 4A). CoQ10 was predicted to bind most strongly at site 2 (XP GlideScore −3.805), which is located between the two

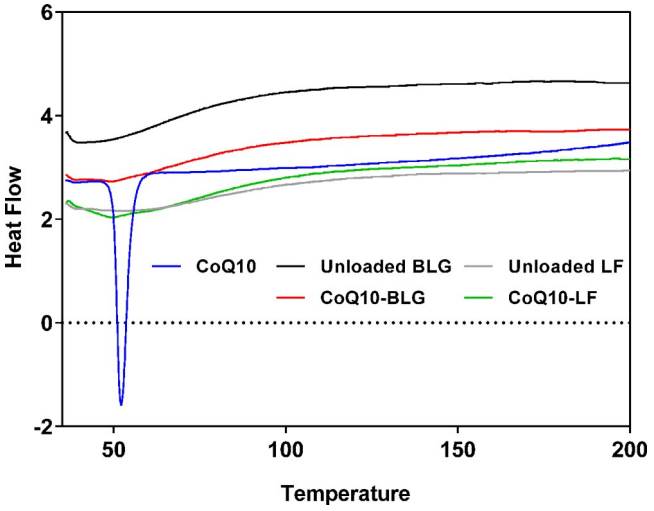

Figure 3. Differential scanning calorimetry (DSC) analysis of CoQ10, blank NPs, and CoQ10NPs.

lobes of LF (Figure 4B). The docking pose of CoQ10 in this site predicted hydrogen bonding of Gln249 and Thr90 with the carbonyl and methoxy oxygens of CoQ10, respectively, and several hydrophobic interactions along the poly isoprenyl tail (Supporting Information Figure S1). This ligand binding site was previously identified in a study that used molecular docking to model the interactions of flavonoids with LF, and participation of Thr90 in hydrogen bonding with the bound ligand (flavonoids) was similarly predicted.[43] When SiteMap was used to examine BLG, only the central pocket was identified as a prospective CoQ10 binding site (SiteScore 0.96). Moreover, this pocket is very narrow and the large structure of CoQ10 did not establish a favorable binding pose in molecular docking (Figure 4C, XP GlideScore 3.378). Overall, *in silico*

https://dx.doi.org/10.1021/acsbiomaterials.0c01354
ACS Biomater. Sci. Eng. 2023, 9, 2846−2856

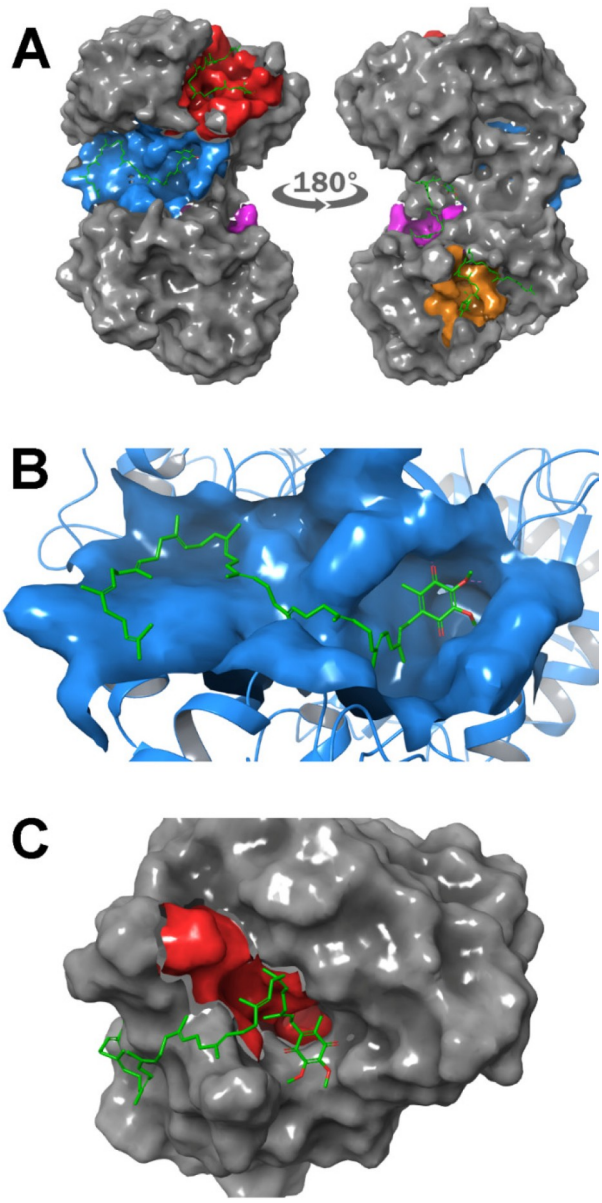

Figure 4. Docking analysis: (A) Glide XP model of CoQ10 (green) docked with four binding sites (red, blue, purple, orange) identified by SiteMap on bovine LF (PDB ID 1BLF). (B) Glide XP model of CoQ10 (green) docked with site 2 identified by SiteMap on bovine LF (PDB ID 1BLF). (C) Glide XP model of CoQ10 (green) docked with BLG (PDB ID 3NPO) showing the large ligand fitting poorly within the narrow binding site (red).

modeling predicts that there are multiple CoQ10 binding sites on the surface of LF, potentially enabling greater loading of CoQ10 on LF compared to BLG, which is predicted to be less capable of binding CoQ10.

3.3. Loading Efficiency and Solubility. Loading efficiency of CoQ10 into the protein NPs was determined by HPLC. The loading efficiency of CoQ10 is higher with CoQ10-LF (86.77 ± 11.15%) compared to CoQ10-BLG (62.79 ± 4.13%) as shown in Table 1. The difference in loading efficiency between BLG and LF may be due to dissimilar protein structures, size, and hydrophobic regions involved in encapsulation of CoQ10. Lower hydrophobic amino acid number (53.4% molar ratio) may have contributed to the low loading efficiency of hydrophobic CoQ10 in BLG.[44] Additionally, poor docking-predicted binding of CoQ10 with BLG (Figure 4B), potentially explaining poor experimental binding and loading capacity. Both CoQ10-LF and CoQ10-BLG revealed significantly improved solubility in deionized water of 300-fold and 60-fold (305.42 μg/mL and 63.32 μg/mL), respectively, compared to control CoQ10, which only had a saturated solubility of 0.21 μg/mL as shown in Figure 5. Although both proteins showed the significantly higher saturated solubility of CoQ10, CoQ10-LF displayed the highest solubility due to stronger and multisite binding of CoQ10 within its hydrophobic pockets. BLG has been extensively used to improve the solubility, stability, and dispersity of many nutraceuticals; however, our results suggest that its utility is perhaps limited, and when it comes to large molecular weight, compounds such as CoQ10 and LF could be a more appropriate choice. Taken together, the above results indicate that LF showed higher encapsulation efficiency, a smaller particle size and PDI of the CoQ10-LF complex, excellent binding with CoQ10, and significantly higher solubility compared to both CoQ10 and CoQ10-BLG.

3.4. *In Vitro* Release and Permeability of CoQ10 from Nanoparticles. The *in vitro* release profile of CoQ10-LF and CoQ10-BLG is shown in Figure 5C as a percentage of cumulative release and amount of CoQ10 released at specific time points. At pH 7.4, up to 30% of CoQ10 was released from CoQ10-LF, whereas only 15% and 7% of CoQ10 was released from CoQ10-BLG and free CoQ10. CoQ10-LF was shown to have a burst release between 30 min and 2 h with up to 23% of CoQ10 released within this time frame. An additional 6% of CoQ10 was released by 12 h, and the release reached a plateau for the subsequent time points. The amount of CoQ10 released in the control was erratic with more than half of the total CoQ10 released in the first 30 min. The better controlled release with CoQ10-LF may be attributed to its improved solubility in deionized water compared to free CoQ10 and CoQ10 encapsulated in BLG. The above results are consistent with our solubility and binding data.

The poor permeability of CoQ10 across GIT is a major contributing factor for its low oral absorption and poor bioavailability.[2,45] The Caco-2 cell monolayer permeation model used in this study was adapted to determine CoQ10 permeability across the small intestinal epithelium.[46] The assessments of transepithelial absorption of CoQ10 (pre dissolved in DMSO 0.5%), CoQ10-BLG, and CoQ10-LF NPs are shown in Figure 5D. CoQ10 alone showed much less absorption via Caco-2 cells (P_{app} ~0.1 × 10^{-6} cm/s) due to its low solubility, which is consistent with previous studies.[2,45] However, higher P_{app} values of 0.39 × 10^{-6} cm/s and 0.48 × 10^{-6} cm/s were observed for CoQ10-BLG and CoQ10-LF NPs in the present study, indicating approximately 2- and 2.5-fold improvement in the permeability using protein nanoparticles compared to predissolved CoQ10. Although improved solubility and stability are thought to be the reason behind improved permeability of hydrophobic compounds from milk-based proteins, further investigation is required to understand the exact mechanism behind enhanced permeation of protein encapsulated CoQ10 NPs.[39] The effect of CoQ10 NPs on TEER before and after treatment is shown in Figure S2. After 2 h, there was not much difference in TEER values of the Caco-2 cell monolayer between the treatments (Figure S2). However, a sudden increase was observed after 24 h, which could be due to replacing the cells with the fresh media after 2 h, indicating cell recovery and reformation of cellular tight junctions, suggesting the inert nature of our formulations.[47]

https://dx.doi.org/10.1021/acsbiomaterials.0c01354
ACS Biomater. Sci. Eng. 2023, 9, 2846−2856

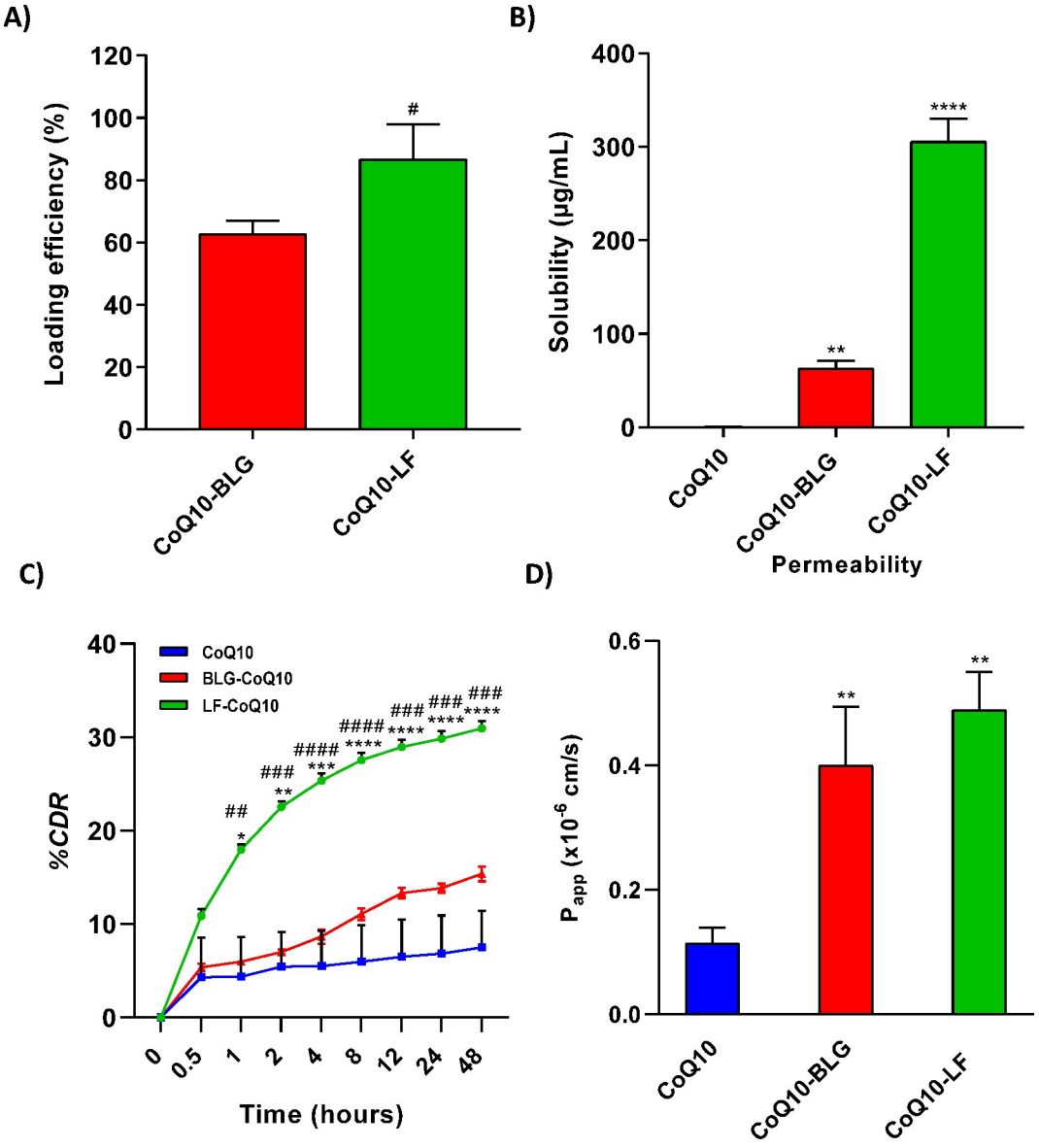

Figure 5. Loading efficiency, solubility, and release profile of Co-Q10 nanoparticles: (A) Loading efficiency of protein NPs for CoQ10-BLG and CoQ10-LF. (B) Solubility of CoQ10-BLG and CoQ10-LF in water ($n = 3$). (C) *In vitro* release at pH 7.4. Percentage of cumulative drug release (% CDR) from CoQ10-LF over 48 h ($n = 3$). (D) Apparent permeability coefficient (P_{app}) of CoQ10-BLG and CoQ10-LF at 2 h in the Caco-2 monolayer (all data are $n = 3$, analyzed by one-way ANOVA, posthoc Tukey's test (*, for comparison with control CoQ10 alone; #, for comparison CoQ10-BLG and CoQ10-LF treated cells). The results were represented as mean ± SD where $^{*,\#}p < 0.05$; $^{**,\#\#}p < 0.0036$; $^{***,\#\#\#}p < 0.0006$, $^{****,\#\#\#\#}p < 0.0001$).

3.5. *In Vitro* Cytotoxicity and Anti-ROS Assay. As shown in Figure 6A, the percentage cell viability was close to 100% for all concentrations of CoQ10-LF equivalent to 5−25 μg/mL CoQ10 when compared to control cells. This means that protein NPs are nontoxic to the macrophages in the range tested (Figure 6A). The inherent production of CoQ10 in the body decreases with age and its level in systemic circulation and tissues decreases. The deficiency of CoQ10 hampers cellular mitochondrial functions producing a varying level of oxidative stresses via reactive oxygen species (ROS) as well as reactive nitrogen species (RNS) as the ROS levels in normal cells are directly dependent on CoQ10. Additionally, CoQ10 localization in the vicinity of mitochondria can battle the cells' oxidative stress.[10] The oxidative stress related to the deficiency of CoQ10 is responsible to a number of cardiovascular, inflammatory, and mitochondrial diseases. Furthermore, it is also reported to possess significant antitumor efficacy when coadministered with doxorubicin nanoparticles and abolished doxorubicin-induced cardiotoxicity.[48] In our case, CoQ10-LF NPs showed significantly reduced ROS levels compared to H_2O_2 stimulated J774A.1 cells for concentrations of 172.9, 230.5, and 288.1 μg/mL (Figure 6D), which were equivalent to 15, 20, and 25 μg/mL CoQ10, respectively. Pure LF showed negligible changes in ROS level, which means that at the tested dose LF has no impact in ROS reduction (Figure 6C), therefore proving that LF does not contribute to synergistic effects in reducing oxidation unlike previously thought. Free CoQ10 (predissolved in up to 0.5% DMSO) appears to reduce the ROS level, however, it does not show any trend in ROS reduction with increasing CoQ10 concentrations. This effect could be due to the effect of DMSO (~0.5%) on the reduction of ROS and not due to CoQ10 as seen in Figure 6B. The reduction of ROS generation was prominent in the case of CoQ10-LF nanoparticles, as compared to the CoQ10 alone (Figure 6). Figure 7 These results were further

https://dx.doi.org/10.1021/acsbiomaterials.0c01354
ACS Biomater. Sci. Eng. 2023, 9, 2846−2856

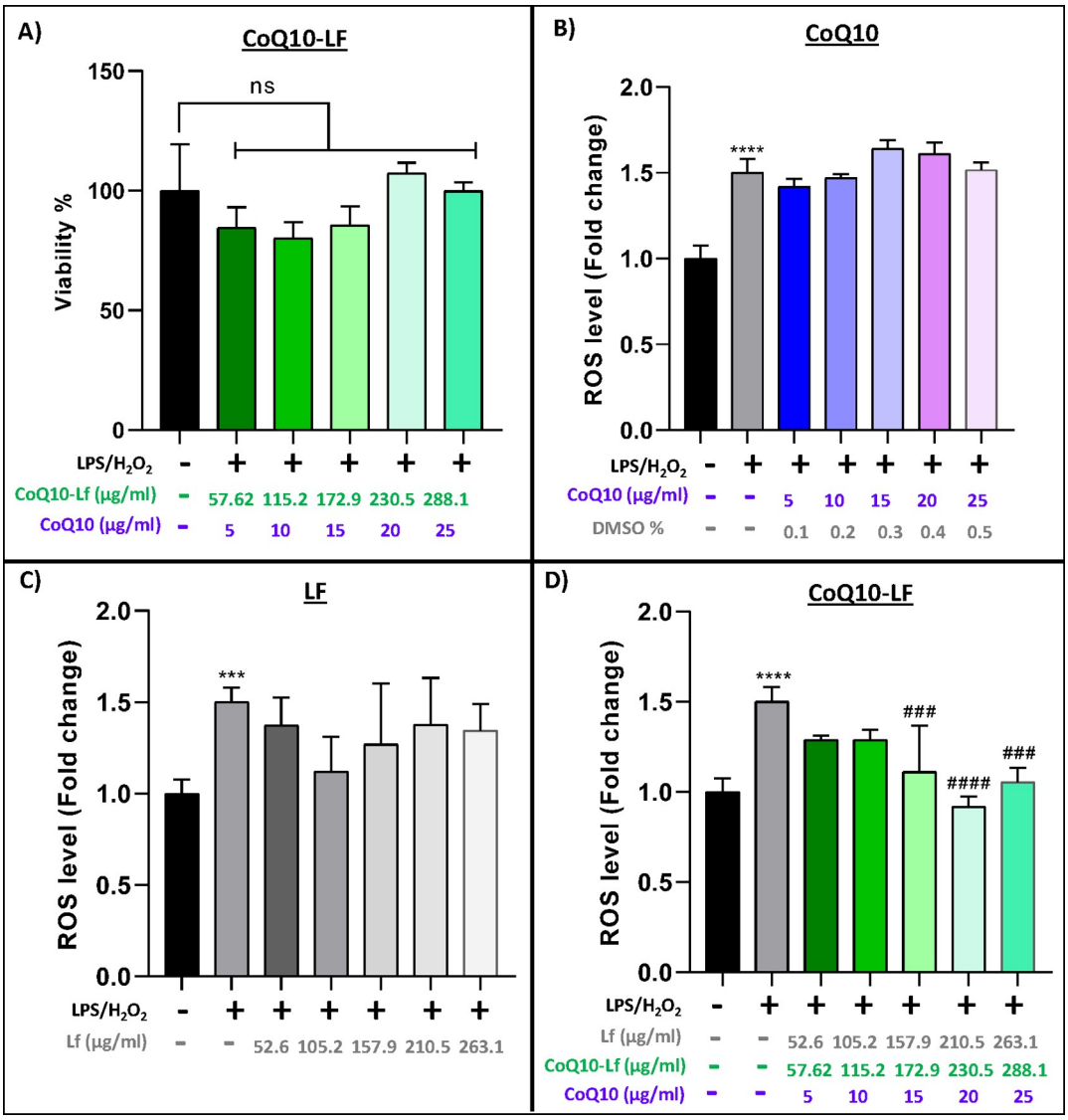

Figure 6. Cell viability with Prestoblue assay and ROS Assay: (A) Percentage of macrophage cell viability (10 000 cells/well) after treatment with different concentration of CoQ10-LF. (B, C, and D) Fold change in Reactive Oxygen Species (ROS) level after 24 h treatment. *Compare to untreated cells as control. In graph C, fold change was normalized against DMSO treated cells, which showed some positive effects. Results are reported as mean ± SD ($n = 3$ separate experiments), $^{*}p < 0.05$, $^{**}p < 0.01$, $^{***}p < 0.001$, $^{****}p < 0.0001$. $^{\#}$Compare to H_2O_2 stimulated control: $^{\#}p < 0.05$, $^{\#\#}p < 0.01$, $^{\#\#\#}p < 0.001$, $^{\#\#\#\#}p < 0.0001$.

corroborated by visualizing the DCHF intensity within J774A.1 cells. As shown in Figure 7, treatment with CoQ10-LF shows a relatively low number of fluorescent cells compared to soluble CoQ10. Therefore, we can conclude that encapsulation of CoQ10 in LF may have enhanced CoQ10 uptake in macrophage cells possibly by improving the solubility and stability of CoQ10 in aqueous media, resulting in a higher antioxidant effect. Overall our finding indicates that CoQ10 nanoencapsulation within protein such as LF significantly improves the antioxidant property *in vitro* in mouse macrophages.

4. CONCLUSION

In this study, we have successfully improved the solubility, dissolution, permeability, and antioxidant properties of CoQ10 by forming a nanocomplex with milk derived proteins. CoQ10 protein nanoparticles were investigated for their physicochemical properties, loading efficiency, solubility, *in vitro* release, and *in vitro* anti-ROS properties. Both CoQ10-NPs (CoQ10-BLG and CoQ10-LF) were shown to have sizes in the nanorange (~250 nm) as opposed to CoQ10, which remained in the micron range. Further, both BLG and LF had excellent encapsulation efficiency with greater than 60% loading efficiency and no crystallization of CoQ10 in CoQ10-NPs, as confirmed with the DSC. Molecular docking studies revealed that CoQ10 bound more strongly to LF (XP GlideScore −3.805) compared to BLG (XP GlideScore 3.378) due to large molecular weight (863 Da) and linear structure of CoQ10. Solubility of CoQ10 was improved 60- and 300-fold, respectively, with CoQ10-BLG and CoQ10-LF. Compared to CoQ10 and CoQ10-BLG, CoQ10-LF displayed significantly higher dissolution at pH 7.4. Further, an *in vitro* permeability assay revealed that both NPs significantly enhanced the CoQ10s apparent permeability coefficient across the Caco-2 monolayer further attesting to our hypothesis. An *in vitro* anti-ROS assay of CoQ10-LF also proved to have a significant reduction of ROS levels compared to predissolved CoQ10 in macrophages for CoQ10 concentrations

https://dx.doi.org/10.1021/acsbiomaterials.0c01354
ACS Biomater. Sci. Eng. 2023, 9, 2846−2856

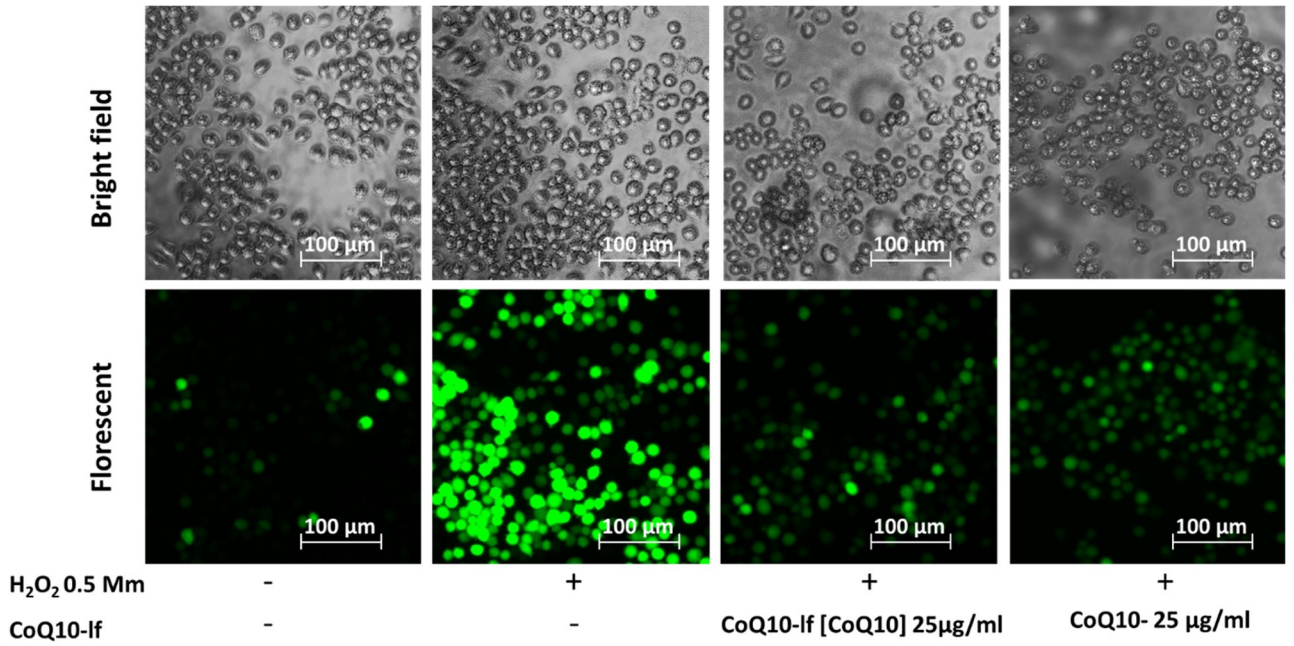

Figure 7. Visualization of cellular ROS level with different CoQ10 treatments: ROS level in macrophage cells as represented by florescent intensity of DCF. Higher florescent intensity means high level of ROS in the cells.

of 15−25 μg/mL and have no harmful effects on cell viability. In summary, our study indicates that encapsulation of CoQ10 using milk proteins improved its solubility, permeability, dissolution profile, and antioxidant properties, making them attractive biomaterials for oral drug delivery of hydrophobic drugs such as CoQ10. Future considerations such as conducting an *in vitro* release at lower pH to mimic gastric secretion, the mechanism of permeation enhancement, and *in vivo* testing is necessary before these formulations can be used clinically.

■ ASSOCIATED CONTENT

Supporting Information

The Supporting Information is available free of charge at https://pubs.acs.org/doi/10.1021/acsbiomaterials.0c01354.

Ligand interaction analysis and TEER recovery (PDF)

■ AUTHOR INFORMATION

Corresponding Authors

Amirali Popat − *School of Pharmacy, The University of Queensland, Brisbane, Queensland 4072, Australia; Mater Research Institute, The University of Queensland, Translational Research Institute, Woolloongabba, Queensland 4102, Australia;* orcid.org/0000-0001-5401-3446; Email: a.popat@uq.edu.au

Tushar Kumeria − *School of Pharmacy, The University of Queensland, Brisbane, Queensland 4072, Australia; School of Materials Science and Engineering, The University of New South Wales, Sydney, New South Wales NSW2052, Australia;* orcid.org/0000-0003-3351-7148; Email: t.kumeria@unsw.edu.au

Authors

Vanessa Jane Banun − *School of Pharmacy, The University of Queensland, Brisbane, Queensland 4072, Australia*

Prarthana Rewatkar − *School of Pharmacy, The University of Queensland, Brisbane, Queensland 4072, Australia*

Zanib Chaudhary − *School of Pharmacy, The University of Queensland, Brisbane, Queensland 4072, Australia*

Zhi Qu − *School of Pharmacy, The University of Queensland, Brisbane, Queensland 4072, Australia*

Taskeen Janjua − *School of Pharmacy, The University of Queensland, Brisbane, Queensland 4072, Australia*

Anuja Patil − *School of Pharmacy, The University of Queensland, Brisbane, Queensland 4072, Australia*

Yuao Wu − *Australian Institute for Bioengineering and Nanotechnology, The University of Queensland, Brisbane, Queensland, Australia; Queensland Micro- and Nanotechnology Centre, Griffith University, Brisbane, Queensland, Australia*

Hang T. Ta − *School of Pharmacy, The University of Queensland, Brisbane, Queensland 4072, Australia; Australian Institute for Bioengineering and Nanotechnology, The University of Queensland, Brisbane, Queensland, Australia; Queensland Micro- and Nanotechnology Centre, Griffith University, Brisbane, Queensland, Australia; School of Environment and Science, Griffith University, Brisbane, Queensland, Australia;* orcid.org/0000-0003-1188-0472

Nidhi Bansal − *School of Pharmacy, The University of Queensland, Brisbane, Queensland 4072, Australia; School of Agriculture and Food Sciences, The University of Queensland, Brisbane, Queensland 4072, Australia*

Jared A. Miles − *School of Pharmacy, The University of Queensland, Brisbane, Queensland 4072, Australia;* orcid.org/0000-0001-5890-7295

Benjamin P. Ross − *School of Pharmacy, The University of Queensland, Brisbane, Queensland 4072, Australia;* orcid.org/0000-0002-1899-8484

Complete contact information is available at: https://pubs.acs.org/10.1021/acsbiomaterials.0c01354

Notes

The authors declare no competing financial interest.

https://dx.doi.org/10.1021/acsbiomaterials.0c01354
ACS Biomater. Sci. Eng. 2023, 9, 2846−2856

■ ACKNOWLEDGMENTS

The authors thank School of Pharmacy, The University of Queensland for the research facilities and financial support. We acknowledge the Australian Microscopy and Microanalysis Research Facility at the Centre for Microscopy and Microanalysis, The University of Queensland. A.P. acknowledges financial support from National Health and Medical Research Council for the Early Career and Career Development Fellowships. T.K. is thankful to the Australian National Health and Medical Research Council for the Early Career Fellowship (GNT1143296), the University of New South Wales (UNSW) for a Scientia Grant, and the Australian Research Council for a discovery project grant (DP200102723).

■ REFERENCES

(1) Ernster, L.; Dallner, G. Biochemical, physiological and medical aspects of ubiquinone function. *Biochim. Biophys. Acta, Mol. Basis Dis.* **1995**, *1271* (1), 195−204.
(2) Zaki, N. M. Strategies for oral delivery and mitochondrial targeting of CoQ10. *Drug Delivery* **2016**, *23* (6), 1868−1881.
(3) Müller, T.; Büttner, T.; Gholipour, A.-F.; Kuhn, W. Coenzyme Q 10 supplementation provides mild symptomatic benefit in patients with Parkinson's disease. *Neurosci. Lett.* **2003**, *341* (3), 201−204.
(4) Shults, C. W.; Flint Beal, M.; Song, D.; Fontaine, D. Pilot trial of high dosages of coenzyme Q10 in patients with Parkinson's disease. *Exp. Neurol.* **2004**, *188* (2), 491−494.
(5) Ayer, A.; Macdonald, P.; Stocker, R. CoQ(1)(0) Function and Role in Heart Failure and Ischemic Heart Disease. *Annu. Rev. Nutr.* **2015**, *35*, 175−213.
(6) Caso, G.; Kelly, P.; McNurlan, M. A.; Lawson, W. E. Effect of Coenzyme Q10 on Myopathic Symptoms in Patients Treated With Statins. *Am. J. Cardiol.* **2007**, *99* (10), 1409−1412.
(7) Palamakula, A.; Soliman, M.; Khan, M. M. Regional permeability of coenzyme Q10 in isolated rat gastrointestinal tracts. *Pharmazie* **2005**, *60* (3), 212−4.
(8) Navas, P.; Villalba, J. M.; de Cabo, R. The importance of plasma membrane coenzyme Q in aging and stress responses. *Mitochondrion* **2007**, *7*, S34−S40.
(9) Takahashi, M.; Takahashi, K. Water-soluble CoQ10 as A Promising Anti-aging Agent for Neurological Dysfunction in Brain Mitochondria. *Antioxidants* **2019**, *8* (3), 61.
(10) Swarnakar, N. K.; Jain, A. K.; Singh, R. P.; Godugu, C.; Das, M.; Jain, S. Oral bioavailability, therapeutic efficacy and reactive oxygen species scavenging properties of coenzyme Q10-loaded polymeric nanoparticles. *Biomaterials* **2011**, *32* (28), 6860−6874.
(11) He, H.; Lu, Y.; Qi, J.; Zhu, Q.; Chen, Z.; Wu, W. Adapting liposomes for oral drug delivery. *Acta Pharm. Sin. B* **2019**, *9* (1), 36−48.
(12) Mauludin, R. *Nanosuspensions of poorly soluble drugs for oral administration [Nanosuspensionen schwerlöslicher Arzneistoffe für orale Applikationen]*; Rainer, H. M., Ed.; Freie Universität Berlin Universitätsbibliothek: Berlin, 2010.
(13) Kommuru, T. R.; Gurley, B.; Khan, M. A.; Reddy, I. K. Self-emulsifying drug delivery systems (SEDDS) of coenzyme Q10: formulation development and bioavailability assessment. *Int. J. Pharm.* **2001**, *212* (2), 233−46.
(14) Xia, S.; Xu, S.; Zhang, X. Optimization in the preparation of coenzyme Q10 nanoliposomes. *J. Agric. Food Chem.* **2006**, *54* (17), 6358−66.
(15) Cheuk, S. Y.; Shih, F. F.; Champagne, E. T.; Daigle, K. W.; Patindol, J. A.; Mattison, C. P.; Boue, S. M. Nano-encapsulation of coenzyme Q10 using octenyl succinic anhydride modified starch. *Food Chem.* **2015**, *174*, 585−90.
(16) Pujara, N.; Jambhrunkar, S.; Wong, K. Y.; McGuckin, M.; Popat, A. Enhanced colloidal stability, solubility and rapid dissolution of resveratrol by nanocomplexation with soy protein isolate. *J. Colloid Interface Sci.* **2017**, *488*, 303−308.
(17) Pujara, N.; Wong, K. Y.; Qu, Z.; Wang, R.; Moniruzzaman, M.; Rewatkar, P.; Kumeria, T.; Ross, B. P.; McGuckin, M.; Popat, A. Oral Delivery of beta-Lactoglobulin-Nanosphere-Encapsulated Resveratrol Alleviates Inflammation in Winnie Mice with Spontaneous Ulcerative Colitis. *Mol. Pharmaceutics* **2021**, *18*, 627.
(18) Liu, W.; Chen, X. D.; Cheng, Z.; Selomulya, C. On enhancing the solubility of curcumin by microencapsulation in whey protein isolate via spray drying. *J. Food Eng.* **2016**, *169*, 189−195.
(19) Penalva, R.; Esparza, I.; Larraneta, E.; González-Navarro, C. J.; Gamazo, C.; Irache, J. M. Zein-Based Nanoparticles Improve the Oral Bioavailability of Resveratrol and Its Anti-inflammatory Effects in a Mouse Model of Endotoxic Shock. *J. Agric. Food Chem.* **2015**, *63* (23), 5603−5611.
(20) Dima, C.; Assadpour, E.; Dima, S.; Jafari, S. M. Bioavailability of nutraceuticals: Role of the food matrix, processing conditions, the gastrointestinal tract, and nanodelivery systems. *Compr. Rev. Food Sci. Food Saf.* **2020**, *19* (3), 954−994.
(21) Chaudhary, Z.; Subramaniam, S.; Khan, G. M.; Abeer, M. M.; Qu, Z.; Janjua, T.; Kumeria, T.; Batra, J.; Popat, A. Encapsulation and Controlled Release of Resveratrol Within Functionalized Mesoporous Silica Nanoparticles for Prostate Cancer Therapy. *Front. Bioeng. Biotechnol.* **2019**, *7*, 225.
(22) Riihimäki, L. H.; Vainio, M. J.; Heikura, J. M. S.; Valkonen, K. H.; Virtanen, V. T.; Vuorela, P. M. Binding of phenolic compounds and their derivatives to bovine and reindeer beta-lactoglobulin. *J. Agric. Food Chem.* **2008**, *56* (17), 7721.
(23) Teng, Z.; Li, Y.; Wang, Q. Insight into curcumin-loaded β-lactoglobulin nanoparticles: incorporation, particle disintegration, and releasing profiles. *J. Agric. Food Chem.* **2014**, *62* (35), 8837.
(24) Reddy, I. M.; Kella, N. K. D.; Kinsella, J. E. Structural and Conformational Basis of the Resistance of β-Lactoglobulin to Peptic and Chymotryptic Digestion. *J. Agric. Food Chem.* **1988**, *36* (4), 737−741.
(25) Adlerova, L.; Bartoskova, A.; Faldyna, M. Lactoferrin: a review. *Vet. Med.* **2008**, *53* (9), 457−468.
(26) Bokkhim, H.; Bansal, N.; Grondahl, L.; Bhandari, B. Physico-chemical properties of different forms of bovine lactoferrin. *Food Chem.* **2013**, *141* (3), 3007−3013.
(27) Bokkhim, H.; Bansal, N.; Grondahl, L.; Bhandari, B. Interactions between different forms of bovine lactoferrin and sodium alginate affect the properties of their mixtures. *Food Hydrocolloids* **2015**, *48*, 38−46.
(28) García-Montoya, I. A.; Cendón, T. S.; Arévalo-Gallegos, S.; Rascón-Cruz, Q. Lactoferrin a multiple bioactive protein: An overview. *Biochim. Biophys. Acta, Gen. Subj.* **2012**, *1820* (3), 226−236.
(29) Liu, F. G.; Sun, C. X.; Yang, W.; Yuan, F.; Gao, Y. X. Structural characterization and functional evaluation of lactoferrin-polyphenol conjugates formed by free-radical graft copolymerization. *RSC Adv.* **2015**, *5* (20), 15641−15651.
(30) Mohan, K. V. P. C.; Gunasekaran, P.; Varalakshmi, E.; Hara, Y.; Nagini, S. In vitro evaluation of the anticancer effect of lactoferrin and tea polyphenol combination on oral carcinoma cells. *Cell Biology International* **2007**, *31* (6), 599−608.
(31) Chen, L.; Subirade, M. Chitosan/β-lactoglobulin core−shell nanoparticles as nutraceutical carriers. *Biomaterials* **2005**, *26* (30), 6041−6053.
(32) Moore, S. A.; Anderson, B. F.; Groom, C. R.; Haridas, M.; Baker, E. N. Three-dimensional structure of diferric bovine lactoferrin at 2.8 angstrom resolution. *J. Mol. Biol.* **1997**, *274* (2), 222−236.
(33) Loch, J.; Polit, A.; Gorecki, A.; Bonarek, P.; Kurpiewska, K.; Dziedzicka-Wasylewska, M.; Lewinski, K. Two modes of fatty acid binding to bovine beta-lactoglobulin-crystallographic and spectroscopic studies. *J. Mol. Recognit.* **2011**, *24* (2), 341−349.
(34) Madhavi Sastry, G.; Adzhigirey, M.; Day, T.; Annabhimoju, R.; Sherman, W. Protein and ligand preparation: parameters, protocols, and influence on virtual screening enrichments. *J. Comput.-Aided Mol. Des.* **2013**, *27* (3), 221−234.
(35) Harder, E.; Damm, W.; Maple, J.; Wu, C.; Reboul, M.; Xiang, J. Y.; Wang, L.; Lupyan, D.; Dahlgren, M. K.; Knight, J. L.; Kaus, J. W.; Cerutti, D. S.; Krilov, G.; Jorgensen, W. L.; Abel, R.; Friesner, R. A.

https://dx.doi.org/10.1021/acsbiomaterials.0c01354
ACS Biomater. Sci. Eng. 2023, 9, 2846−2856

OPLS3: A Force Field Providing Broad Coverage of Drug-like Small Molecules and Proteins. *J. Chem. Theory Comput.* **2016**, *12* (1), 281−296.
(36) Halgren, T. A. Identifying and characterizing binding sites and assessing druggability. *J. Chem. Inf. Model.* **2009**, *49* (2), 377−89.
(37) Friesner, R. A.; Murphy, R. B.; Repasky, M. P.; Frye, L. L.; Greenwood, J. R.; Halgren, T. A.; Sanschagrin, P. C.; Mainz, D. T. Extra precision glide: docking and scoring incorporating a model of hydrophobic enclosure for protein-ligand complexes. *J. Med. Chem.* **2006**, *49* (21), 6177−96.
(38) Beloqui, A.; Coco, R.; Memvanga, P. B.; Ucakar, B.; des Rieux, A.; Préat, V. pH-sensitive nanoparticles for colonic delivery of curcumin in inflammatory bowel disease. *Int. J. Pharm.* **2014**, *473* (1−2), 203−212.
(39) Li, M.; Cui, J.; Ngadi, M. O.; Ma, Y. Absorption mechanism of whey-protein-delivered curcumin using Caco-2 cell monolayers. *Food Chem.* **2015**, *180*, 48−54.
(40) Hubatsch, I.; Ragnarsson, E. G. E.; Artursson, P. Determination of drug permeability and prediction of drug absorption in Caco-2 monolayers. *Nat. Protoc.* **2007**, *2* (9), 2111−2119.
(41) Dhawan, A.; Sharma, V. Toxicity assessment of nanomaterials: methods and challenges. *Anal. Bioanal. Chem.* **2010**, *398* (2), 589−605.
(42) Fir, M. M.; Smidovnik, A.; Milivojevic, L.; Zmitek, J.; Prosek, M. Studies of CoQ10 and cyclodextrin complexes: solubility, thermo- and photo-stability. *J. Inclusion Phenom. Mol. Recognit. Chem.* **2009**, *64* (3), 225−232.
(43) Huang, J.; Liu, Z.; Ma, Q.; He, Z.; Niu, Z.; Zhang, M.; Pan, L.; Qu, X.; Yu, J.; Niu, B. Studies on the Interaction between Three Small Flavonoid Molecules and Bovine Lactoferrin. *BioMed Res. Int.* **2018**, *2018*, 7523165.
(44) Chen, J.; Zheng, J.; McClements, D. J.; Xiao, H. Tangeretin-loaded protein nanoparticles fabricated from zein/β-lactoglobulin: Preparation, characterization, and functional performance. *Food Chem.* **2014**, *158*, 466−472.
(45) Itagaki, S.; Ochiai, A.; Kobayashi, M.; Sugawara, M.; Hirano, T.; Iseki, K. Grapefruit juice enhance the uptake of coenzyme Q10 in the human intestinal cell-line Caco-2. *Food Chem.* **2010**, *120* (2), 552−555.
(46) Fortuna, A.; Alves, G.; Falcão, A. Importance of permeability screening in drug discovery process: PAMPA, Caco-2 and rat everted gut assays. *Current Topics in Pharmacology* **2007**, *11*, 63−86.
(47) Wang, M.; Zhang, Y.; Sun, B.; Sun, Y.; Gong, X.; Wu, Y.; Zhang, X.; Kong, W.; Chen, Y. Permeability of exendin-4-loaded chitosan nanoparticles across MDCK cell monolayers and rat small intestine. *Biol. Pharm. Bull.* **2014**, *37* (5), 740−7.
(48) Swarnakar, N. K.; Thanki, K.; Jain, S. Effect of co-administration of CoQ10-loaded nanoparticles on the efficacy and cardiotoxicity of doxorubicin-loaded nanoparticles. *RSC Adv.* **2013**, *3* (34), 14671−14685.

https://dx.doi.org/10.1021/acsbiomaterials.0c01354
ACS Biomater. Sci. Eng. 2023, 9, 2846−2856